

Higgs Portal Vector Dark Matter : Revisited

Seungwon Baek,^a P. Ko,^a Wan-Il Park^a and Eibun Senaha^a

^a*School of Physics, KIAS,
Seoul 130-722, Korea*

E-mail: sbaek1560@gmail.com, pko@kias.re.kr, wipark@kias.re.kr,
senaha@kias.re.kr

ABSTRACT: We revisit the Higgs portal vector dark matter model including a hidden sector Higgs field that generates the mass of the vector dark matter. The model becomes renormalizable and has two scalar bosons, the mixtures of the SM Higgs and the hidden sector Higgs bosons. The strong bound from direct detection such as XENON100 is evaded due to the cancellation mechanism between the contributions from two scalar bosons. As a result, the model becomes still viable in large range of dark matter mass, contrary to some claims in the literature. The Higgs property is also affected, the signal strengths for the Higgs boson search being universally suppressed relative to the SM value.

KEYWORDS:

Contents

1	Introduction	1
2	The model	2
3	Phenomenology	3
3.1	Dark Matter Phenomenology	3
3.2	Collider Phenomenology	5
4	Vacuum stability and perturbativity of Higgs quartic couplings	9
5	Conclusions	11
A	One-loop β functions of Higgs quartic couplings	12

1 Introduction

The so-called Higgs portal cold dark matter (CDM) model is an interesting possibility for the nonbaryonic dark matter of the universe. The dark matter fields are assumed to be the SM gauge singlets, and could be a scalar (S), a singlet fermion (ψ) or a vector boson (V) depending on their spin. The Lagrangian of these CDM's are usually taken as [1]

$$\mathcal{L}_{\text{scalar}} = \frac{1}{2}\partial_\mu S \partial^\mu S - \frac{1}{2}m_S^2 S^2 - \frac{\lambda_{HS}}{2}H^\dagger H S^2 - \frac{\lambda_S}{4}S^4 \quad (1.1)$$

$$\mathcal{L}_{\text{fermion}} = \bar{\psi}[i\gamma \cdot \partial - m_\psi]\psi - \frac{\lambda_{H\psi}}{\Lambda}H^\dagger H \bar{\psi}\psi \quad (1.2)$$

$$\mathcal{L}_{\text{vector}} = -\frac{1}{4}V_{\mu\nu}V^{\mu\nu} + \frac{1}{2}m_V^2 V_\mu V^\mu + \frac{1}{4}\lambda_V(V_\mu V^\mu)^2 + \frac{1}{4}\lambda_{HV}H^\dagger H V_\mu V^\mu. \quad (1.3)$$

Dark matter fields (S, ψ, V) are assumed to be odd under new discrete Z_2 symmetry: $(S, \psi, V) \rightarrow -(S, \psi, V)$ in order to guarantee the stability of CDM. This symmetry removes the kinetic mixing between the $V_{\mu\nu}$ and the $U(1)_Y$ gauge field $B^{\mu\nu}$, making V stable.

The scalar CDM model (1.1) is fine, as long as Z_2 symmetry is unbroken. The model is renormalizable and can be considered to high energy scale as long as the Landau pole is not hit. On the other hand, the other two cases have problems.

Let us first consider the fermionic CDM model (1.2). This model is nonrenormalizable, and has to be UV completed. The simplest way to achieve the UV completion of (1.2) is to introduce a real singlet scalar field as proposed in Ref. [2, 3] by some of us. We observed that there are two Higgs-like scalar bosons which interfere destructively in the spin-independent cross section of the singlet fermion CDM on nucleon. The strong constraint from direct detection experiments such as XENON100 [4] or CDMS [5] can be relaxed by a significant

amount, unlike the claim made in literatures [1] based on the effective Lagrangian (1.2). The decoupling of the 2nd scalar boson occurs rather slowly, since the mass mixing between the SM Higgs boson and the new singlet scalar is due to the dim-2 operator. Also the mixing between two scalar bosons makes the signal strength of two physical Higgs-like bosons less than one, and make it difficult to detect both of them at the LHC. Since there is now an evidence for a new boson at 125 GeV at the LHC [6, 7], the 2nd scalar boson in the singlet fermion DM model is very difficult to observe at the LHC because its signal strength is less than 0.3 [3, 8]. Also an extra singlet scalar saves the vacuum instability for $m_H = 125$ GeV [8–10]. The electroweak (EW) vacuum can be still stable upto Planck scale even for $m_H = 125$ GeV [8]. These phenomena would be very generic in general hidden sector DM models [11]. In short, it is very important to consider a renormalizable model when one considers the phenomenology of a singlet fermion CDM.

Now let us turn to the Higgs portal vector dark matter described by (1.3) [1]. This model is very simple, compact and seemingly renormalizable since it has only dim-2 and dim-4 operators. However, it is not really renormalizable and violates unitarity, just like the intermediate vector boson model for massive weak gauge bosons before Higgs mechanism was developed. The Higgs portal VDM model based on (1.3) is a sort of an effective lagrangian which has to be UV completed. It lacks including the dark Higgs field, $\varphi(x)$, that would mix with the SM Higgs field, $h(x)$. Therefore the model (1.3) does not capture dark matter or Higgs boson phenomenology correctly. It is the purpose of this work to propose a simple UV completion of the model (1.3), and deduce the correct phenomenology of vector CDM and two Higgs-like scalar bosons. Qualitative aspects of our model are similar to those presented in Ref.s [3, 8], although there are some quantitative differences due to the vector nature of the CDM.

This work is organized as follows. In Sec. 2, we define the model by including the hidden sector Higgs field that generates the vector dark matter mass by the usual Higgs mechanism. Then we present dark matter and collider phenomenology in the following section. The vacuum structure and the vacuum stability issues are discussed in Sec. 4, and the results are summarized in Sec. 5.

2 The model

Let us consider a vector boson dark matter, X_μ , which is assumed to be a gauge boson associated with Abelian dark gauge symmetry $U(1)_X$. The simplest model will be without any matter fields charged under $U(1)_X$ except for a complex scalar, Φ , whose VEV will generate the mass for X_μ [12]:

$$\begin{aligned} \mathcal{L}_{VDM} = & -\frac{1}{4}X_{\mu\nu}X^{\mu\nu} + (D_\mu\Phi)^\dagger(D^\mu\Phi) - \lambda_\Phi\left(\Phi^\dagger\Phi - \frac{v_\Phi^2}{2}\right)^2 \\ & - \lambda_{H\Phi}\left(H^\dagger H - \frac{v_H^2}{2}\right)\left(\Phi^\dagger\Phi - \frac{v_\Phi^2}{2}\right), \end{aligned} \quad (2.1)$$

in addition to the SM lagrangian. The covariant derivative is defined as

$$D_\mu\Phi = (\partial_\mu + ig_X Q_\Phi X_\mu)\Phi,$$

where $Q_\Phi \equiv Q_X(\Phi)$ is the $U(1)_X$ charge of Φ and we will take $Q_\Phi = 1$ throughout the paper.

Assuming that the $U(1)_X$ -charged complex scalar Φ develops a nonzero VEV, v_Φ , and thus breaks $U(1)_X$ spontaneously,

$$\Phi = \frac{1}{\sqrt{2}} (v_\Phi + \varphi(x)).$$

Therefore the Abelian vector boson X_μ get mass $m_X^2 = g_X^2 Q_\Phi^2 v_\Phi^2$, and the hidden sector Higgs field (or dark Higgs field) $\varphi(x)$ will mix with the SM Higgs field $h(x)$ through Higgs portal of the $\lambda_{H\Phi}$ term. It is straightforward to derive the Feynman rules from this Lagrangian after the $U(1)_X$ and EW symmetries are spontaneously broken.

3 Phenomenology

3.1 Dark Matter Phenomenology

The observed present cold dark matter density, $\Omega_{\text{CDM}} h^2 \simeq 0.1123 \pm 0.0035$ [13], is approximately related to the thermally averaged annihilation cross section at freeze-out temperature, $\langle \sigma v \rangle_{\text{fz}}$, as

$$\Omega_{\text{CDM}} h^2 = \frac{3 \times 10^{-27} \text{cm}^3/\text{s}}{\langle \sigma v \rangle_{\text{fz}}}. \quad (3.1)$$

So we require $\langle \sigma v \rangle_{\text{fz}} \approx 3 \times 10^{-26} \text{cm}^3/\text{s}$ to obtain the correct relic density. We have used the micrOmegas v.2.4.5 [14] to calculate thermal relic density and direct detection cross section of the VDM in our model.

In Fig. 1 we show the thermal relic density as a function of the dark matter mass, M_X . For this plot we fixed $m_1 = 125 \text{ GeV}$, $m_2 = 150 \text{ GeV}$, $\alpha = \pi/4$ and the purple (blue) line corresponds to $g_X = 0.05$ (0.5). We can see two resonance dips at $M_X = m_i/2$ ($i = 1, 2$). The VDMs can annihilate into the SM particles in the S-wave state, which is different from the singlet fermionic dark matter case studied in [3] where the annihilation occurs in the P-wave state. As a result the annihilation cross section for the vector dark matter is generally $\mathcal{O}(10 - 100)$ larger than that of the SFDM. And the current relic density can be explained more easily even at non-resonance region. (See the blue line in Fig. 1.)

One important effect when considering the full theory, which we found in Ref. [3], is that a generic cancellation occurs in the dark matter and nucleon scattering amplitude, which can not be observed in the effective lagrangian approach.¹ This is because the transformation matrix between the interaction eigenstates and the mass eigenstates in the scalar sector is an orthogonal matrix. The dark matter and nucleon elastic scattering cross

¹In general the cancellation mechanism can also work in the annihilation process for the relic density. However, the different decay widths for the H_1 and H_2 and/or other processes such as annihilations into scalar particle pairs makes it less effective than in the direct detection process. As a result, the annihilation process and the direct detection process are not strictly proportional to each other in our scenario.

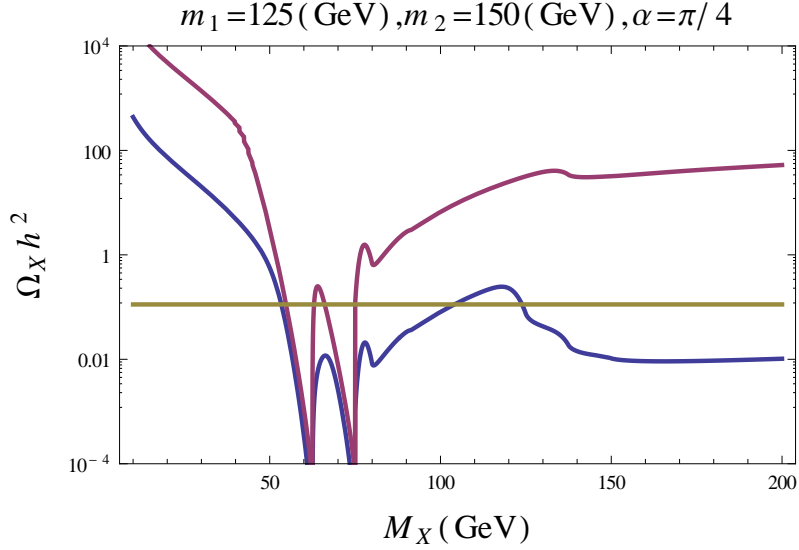


Figure 1. The thermal relic density $\Omega_X h^2$ of the vector dark matter as a function of the dark matter mass, M_X . For this plot we fixed $m_1 = 125$ GeV, $m_2 = 150$ GeV, $\alpha = \pi/4$ and the purple (blue) line corresponds to $g_X = 0.05$ (0.5). The horizontal line is the central value of the current relic density $\Omega_X h^2 = 0.1123$ [13].

section is proportional to the following factor²:

$$\sigma_p \propto \left| \sum_{i=1,2} \frac{O_{hi} O_{\varphi i}}{q^2 - m_i^2} \right|^2, \quad (3.3)$$

where q is the momentum transfer of the dark matter. When $m_1 \approx m_2$ or $|q^2| \gg m_i^2$, we have $\sigma_p \approx 0$ due to the orthogonality of the mixing matrix O . This cancellation phenomenon is quite similar to the GIM-mechanism [15] in the quark (or lepton) flavor violating neutral current processes. In Fig. 2, we show the excluded region in the (g_X, α) -plane by the non-observation of dark matter by the XENON100 which currently gives the strongest bound on the dark matter direct detection cross section [4]. Each colored region is excluded by XENON100 direct detection experiment for the m_2 value given in the plot. We fixed $M_X = 70$ GeV, $m_1 = 125$ GeV for the plot. The black line corresponds to $\Omega_X h^2 = 0.1123$ with $m_2 = 135$ GeV. So the relic density is consistent with the XENON100 experiment. The entire region is also allowed by the electroweak precision S, T, U -parameters at 99% confidence level for this choice of parameter space.

The predictions of our model on the S, T parameters assuming $U = 0$ are shown in Fig. 3 for the choices $(m_1, m_2) = (25, 125), (50, 125), (75, 125), (100, 125), (125, 125)$,

²The transformation matrix O is defined as

$$\begin{pmatrix} h \\ \varphi \end{pmatrix} = O \begin{pmatrix} H_1 \\ H_2 \end{pmatrix} \equiv \begin{pmatrix} c_\alpha & s_\alpha \\ -s_\alpha & c_\alpha \end{pmatrix} \begin{pmatrix} H_1 \\ H_2 \end{pmatrix} \quad (3.2)$$

where $s_\alpha(c_\alpha) \equiv \sin \alpha(\cos \alpha)$, h, φ are the interaction eigenstates and $H_i (i = 1, 2)$ are the mass eigenstates.

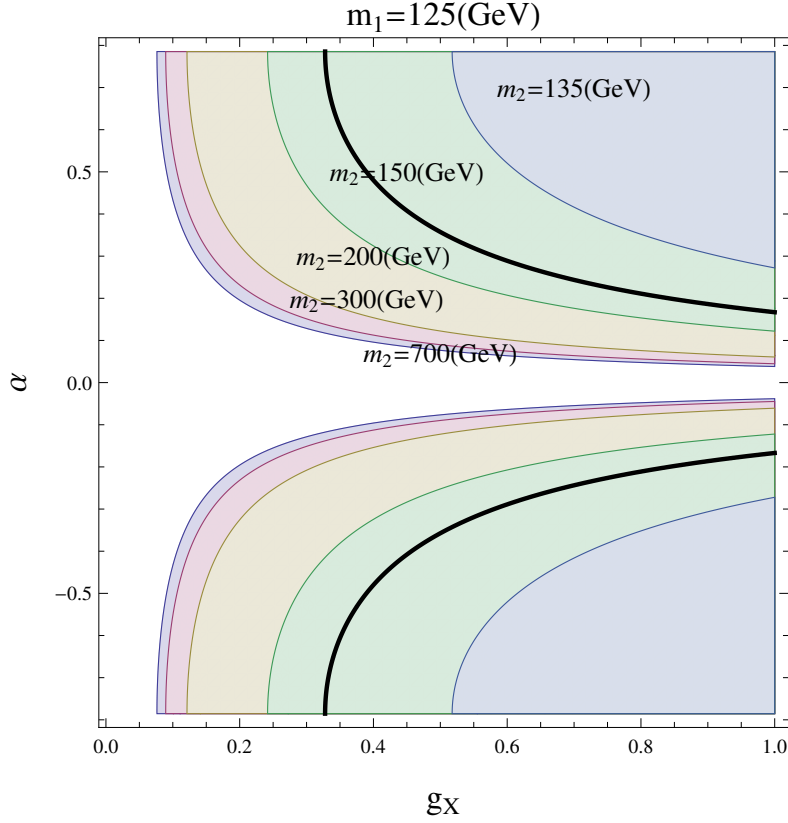


Figure 2. The excluded region in the (g_X, α) -plane. Each colored region is excluded by XENON100 direct detection experiment for the m_2 value given in the plot. We fixed $M_X = 70$ GeV, $m_1 = 125$ GeV. The black line corresponds to $\Omega_X h^2 = 0.1123$ with $m_2 = 135$ GeV. So the relic density is consistent with the XENON100 experiment. The entire region is also allowed by the S, T, U -parameters at 99% confidence level.

(125, 250), (125, 500), (125, 750) (GeV). The green (red) dots are for $\alpha = 45^\circ (20^\circ)$. The thick black line is the prediction of the SM with the m_H in the range [125, 720] (GeV). The ellipses represent 68, 95, 99% CL experimental lines from inside out.

3.2 Collider Phenomenology

Since the scalar sector is extended, the Higgs phenomenology is different from that of the SM. In this subsection we study the possibility that the second Higgs which our model predicts could be discovered at the LHC. We will also see that the combination of the collider signatures and the DM direct searches is robust enough to exclude or confirm our model in the on-going LHC and the next generation DM direct detection experiments.

The signal strength of a scalar boson $H_{i=1,2}$ defined as

$$r_i \equiv \frac{\sigma(pp \rightarrow H_i) B(H_i \rightarrow X)}{[\sigma(pp \rightarrow H_i) B(H_i \rightarrow X)]^{\text{SM}}} \quad (3.4)$$

can be measured at the LHC. Here $i = 1, 2$ and X is a specific SM final state which the scalar boson H_i can decay into. In our model it can be written in terms of $\Gamma_i^{\text{tot, SM}}$ ($i = 1, 2$)

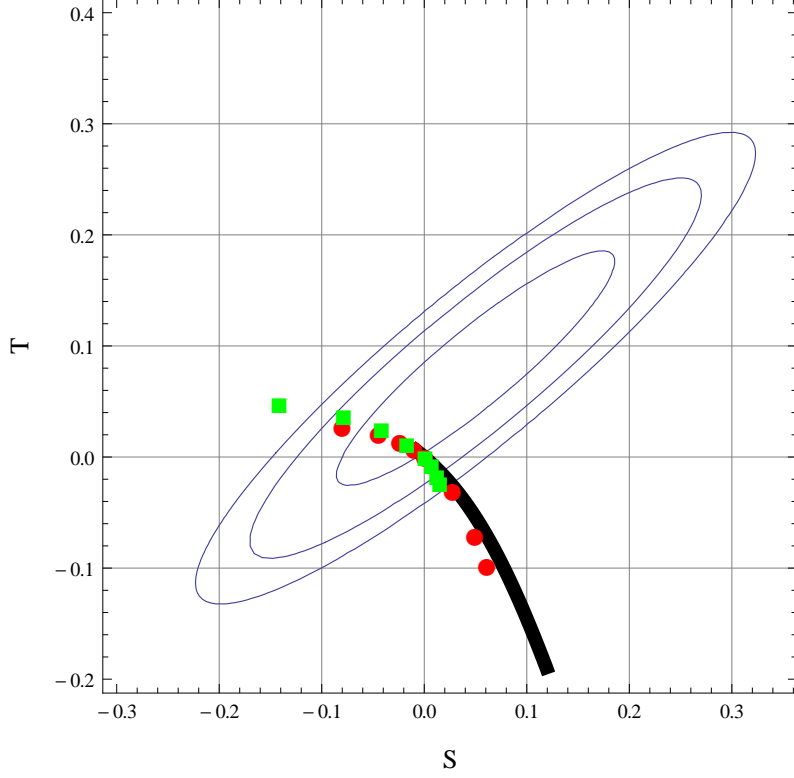


Figure 3. The predictions of (S, T) -parameters in our model for $(m_1, m_2) = (25, 125), (50, 125), (75, 125), (100, 125), (125, 125), (125, 250), (125, 500), (125, 750)$ (GeV). The green (red) dots are for $\alpha = 45^\circ (20^\circ)$. The thick black line is the prediction of the SM with the m_H in the range $[125, 720]$ (GeV). The ellipses represent 68, 95, 99% CL experimental lines from inside out.

which is the total decay width of H_i in the SM assuming H_i is a pure SM Higgs and Γ_i^{tot} which is the total decay width of H_i in our model [3, 8]:

$$r_i = O_{hi}^4 \frac{\Gamma_i^{\text{tot,SM}}}{\Gamma_i^{\text{tot}}}, \quad (3.5)$$

where $O_{h1} = c_\alpha, O_{h2} = s_\alpha$. The total decay widths can be decomposed as

$$\begin{aligned} \Gamma_1^{\text{tot}} &= c_\alpha^2 \Gamma_1^{\text{tot,SM}} + s_\alpha^2 \Gamma_1^{\text{tot,hid}}, \\ \Gamma_2^{\text{tot}} &= s_\alpha^2 \Gamma_2^{\text{tot,SM}} + c_\alpha^2 \Gamma_2^{\text{tot,hid}} + \Gamma(H_2 \rightarrow H_1 H_1), \end{aligned} \quad (3.6)$$

where $\Gamma_i^{\text{tot,hid}}$ is the total decay width of H_i into the hidden sector assuming H_i is a pure SM-singlet scalar. The channel $H_2 \rightarrow H_1 H_1$ opens when $m_2 > 2m_1$. From the eqs. (3.5) and (3.6) it is obvious that $r_i < 1$ in our model. Therefore if the excess of the signal strength in some channels like $H \rightarrow \gamma\gamma$ above the SM prediction at the LHC remains in the future data, our model will either be excluded or need to be extended (two Higgs doublet portal to a hidden sector dark matter, for example). In fact we find $r < 0.3$ for the second Higgs boson, when we impose the observed new boson at 125 GeV as one of the Higgs bosons in our model.

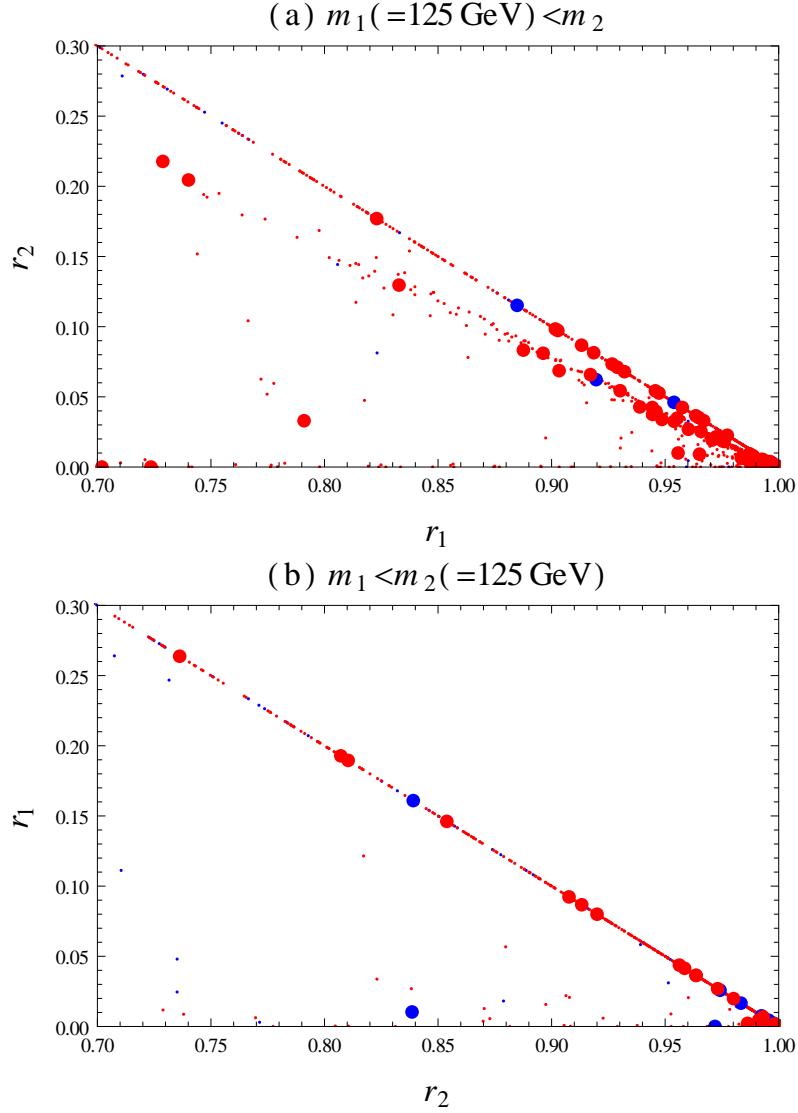


Figure 4. The scattered plot in (a) (r_1, r_2) for $m_1(= 125 \text{ GeV}) < m_2$ and (b) (r_2, r_1) for $m_1 < m_2(= 125 \text{ GeV})$. The big (small) points (do not) satisfy the WMAP relic density constraint within 3σ , while the red-(blue-)colored points can (cannot) be probed at the planned XENON1T direct detection experiment.

The correlation between r_1 and r_2 can be seen in Fig. 4 where we show only the region $r_1 > 0.7$. For this plot we scanned the parameters g_X , M_X , α , m_2 in the range, $0 < g_X < 1$, $10 \text{ GeV} < M_X < 1000 \text{ GeV}$, $-\pi/2 < \alpha < \pi/2$, $m_1(= 125 \text{ GeV}) < m_2 < 2000 \text{ GeV}$ for the panel (a), and $10 \text{ GeV} < m_1 < m_2(= 125 \text{ GeV})$ for the panel (b). All the points pass the constraints: $\Omega_X h^2 < 0.1228$ (the 3σ upper bound of the relic density), the upper bound on the XENON100 direct detection cross section, and the bound on the S, T -parameters at 99% CL. The big (small) points (do not) satisfy the WMAP relic density constraint within 3σ , while the red-(blue-)colored points can (cannot) be probed at the planned XENON1T direct detection experiment [16]. In both plots, the big red points on the straight line,

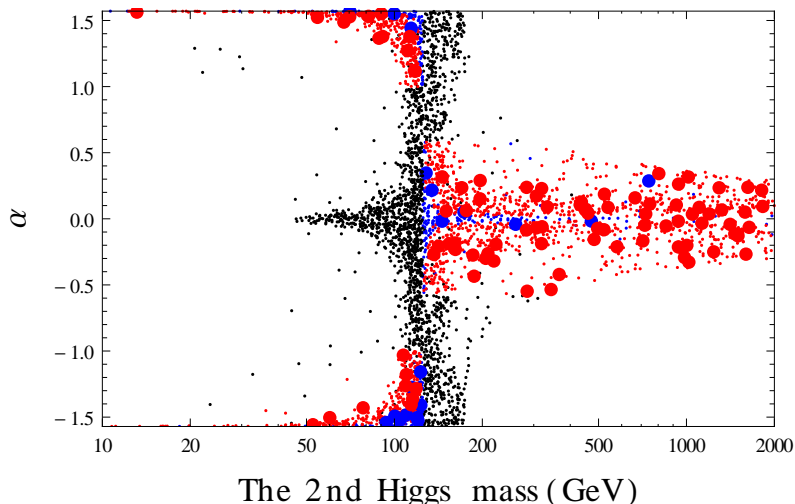


Figure 5. The allowed mixing angle α as a function of the second Higgs mass. We fixed the SM-like Higgs mass to be 125 GeV. The big (small) points (do not) satisfy the WMAP relic density constraint within 3σ , while the red-(blue-)colored points can (cannot) be probed at the planned XENON1T experiment. The black points are excluded by the LHC Higgs search, *i.e.* $r < 0.7$.

$r_1 + r_2 = 1$, are those with $H_i \rightarrow XX$ and $H_2 \rightarrow H_1 H_1$ suppressed. In the panel (a), the sizable contribution from the $H_2 \rightarrow H_1 H_1$ channel allows the big red points below the $r_1 + r_2 = 1$ line.

In Fig. 5, we show the allowed mixing angle α as a function of the second Higgs mass. We fixed the SM-like Higgs mass to be 125 GeV. The big (small) points (do not) satisfy the WMAP relic density constraint within 3σ , while the red-(blue-)colored points can (cannot) be probed at the planned XENON1T experiment. The black points are excluded by the LHC Higgs search, *i.e.* $r < 0.7$. We can see the maximal mixing angle $\alpha = \pi/4$ (black points near $m_2 \approx 125$ GeV) is excluded by the LHC Higgs search. Also the light scalar with mass less than 125 GeV, if exists, should be singlet-like.

In Fig. 6, we show a scattered plot of σ_p as a function of M_X . The big (small) points (do not) satisfy the WMAP relic density constraint within 3σ , while the red-(black-)colored points gives $r_1 > 0.7$ ($r_1 < 0.7$). The Gray region is excluded by the XENON100 experiment. The dashed line denotes the sensitivity of the next XENON experiment, XENON1T. We note that many points are still allowed by the WMAP relic density constraint, the XENON100 direct detection experiment, and also by the constraint $r_1 > 0.7$ which is in the ball park of the LHC Higgs search bound. On the other hand, the effective field theory approach considered in Ref.s [1] strongly constrains the vector dark matter scenario. We can also see that there is no point below about $M_X \approx 50$ GeV in Fig. 6 (a). It is because the Higgs exchanged dark matter annihilation channel does not allow the resonance and the relic density is larger than the WMAP measurement. Most of the big red points are within the reach of the XENON1T sensitivity, and our model can be tested in the next generation dark matter detection experiment.

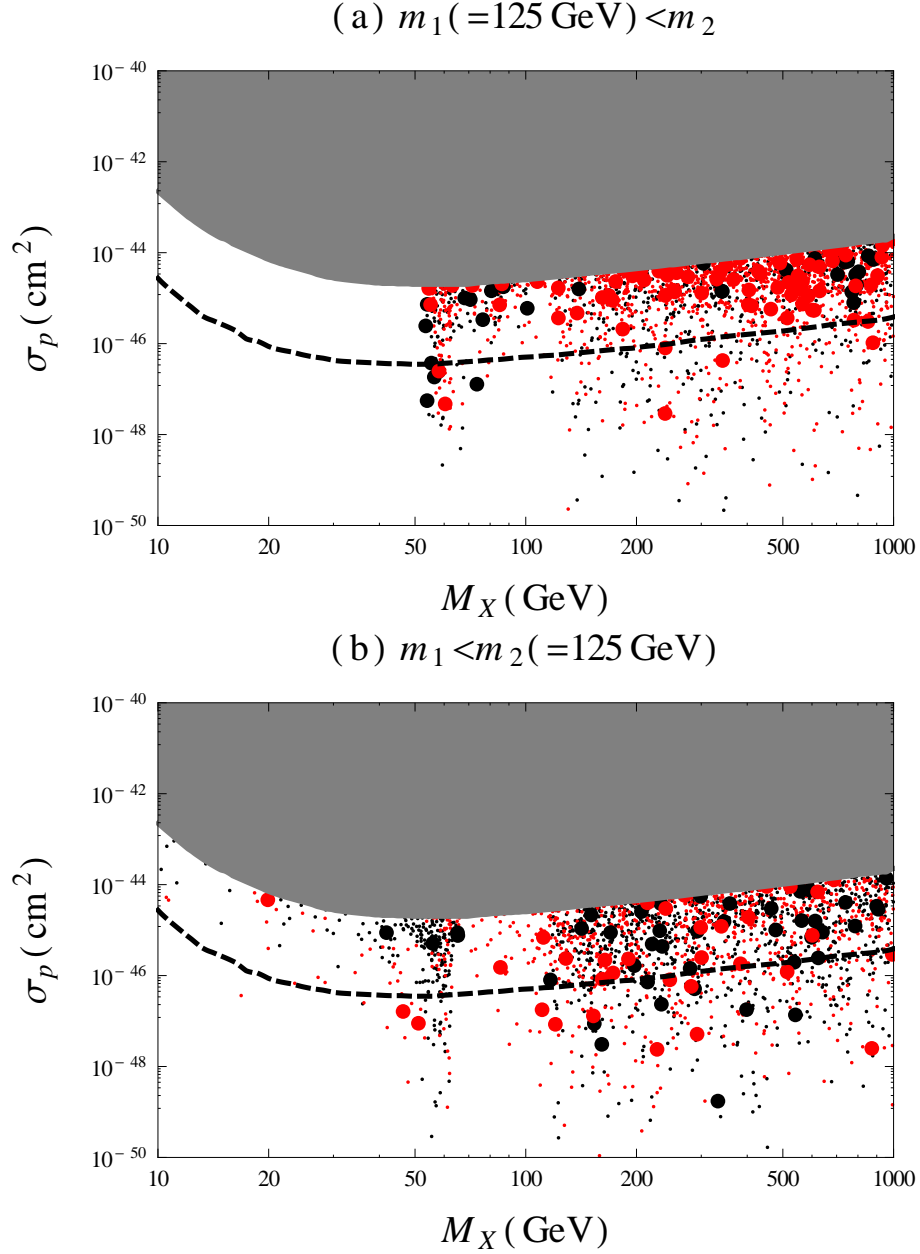


Figure 6. The scattered plot of σ_p as a function of M_X . The big (small) points (do not) satisfy the WMAP relic density constraint within 3σ , while the red-(black-)colored points gives $r_1 > 0.7$ ($r_1 < 0.7$). The gray region is excluded by the XENON100 experiment. The dashed line denotes the sensitivity of the next XENON experiment, XENON1T.

4 Vacuum stability and perturbativity of Higgs quartic couplings

In this section, we analyze vacuum stability and perturbativity of Higgs quartic couplings. To make the Higgs potential be bounded-from-below, we require

$$\lambda_H > 0, \quad \lambda_\Phi > 0, \quad -2\sqrt{\lambda_H \lambda_\Phi} < \lambda_{H\Phi}, \quad (4.1)$$

where the last condition applies for $\lambda_{H\Phi} < 0$. We also require

$$\det M_{\text{Higgs}}^2 = \det \begin{pmatrix} 2\lambda_H v_H^2 & \lambda_{H\Phi} v_H v_\Phi \\ \lambda_{H\Phi} v_H v_\Phi & 2\lambda_\Phi v_\Phi^2 \end{pmatrix} = (4\lambda_H \lambda_\Phi - \lambda_{H\Phi}^2) v_H^2 v_\Phi^2 > 0. \quad (4.2)$$

Since there is additional direction of Φ , the Higgs potential can have minima other than our EW vacuum. In the following, we investigate whether the EW vacuum is global or not. We closely follow the analysis done in Ref. [8].

The tree-level effective potential takes the $U(1)_X$ symmetric form

$$V_0(\varphi_H, \varphi_\Phi) = \frac{\lambda_H}{4}(\varphi_H^4 - 2v_H^2 \varphi_H^2) + \frac{\lambda_\Phi}{4}(\varphi_\Phi^4 - 2v_\Phi^2 \varphi_\Phi^2) + \frac{\lambda_{H\Phi}}{4}(\varphi_H^2 \varphi_\Phi^2 - \varphi_H^2 v_\Phi^2 - v_H^2 \varphi_\Phi^2), \quad (4.3)$$

where φ_H and φ_Φ are spacetime-independent classical fields. Unlike the general Higgs potential, only nontrivial phase may be the I-phase which is defined by a minimum of $V_0(0, \varphi_\Phi)$. Such a minimum is given by

$$\bar{v}_\Phi = \pm \sqrt{v_\Phi^2 + \frac{\lambda_{H\Phi}}{2\lambda_\Phi} v_H^2}. \quad (4.4)$$

The differences of vacuum energies of the I- and the EW phases is

$$\begin{aligned} V_0^{(I)}(0, \bar{v}_\Phi) - V_0^{(\text{EW})}(v_H, v_\Phi) &= \frac{\lambda_H}{4} v_H^4 + \frac{\lambda_{H\Phi}}{4} v_H^2 v_\Phi^2 - \frac{\lambda_\Phi}{4} (\bar{v}_\Phi^4 - v_\Phi^4) \\ &= \frac{1}{16\lambda_\Phi} (4\lambda_H \lambda_\Phi - \lambda_{H\Phi}^2) v_H^4, \end{aligned} \quad (4.5)$$

where we have used Eq. (4.4) in the second line. Therefore, as long as Eqs. (4.1) and (4.2) are satisfied, the EW vacuum is always the global minimum. Note that this is not the case for the generic Higgs potential [8].

Although the EW vacuum is stable at the EW scale, its stability up to Planck scale ($M_{\text{Pl}} \simeq 1.22 \times 10^{19}$ GeV) is nontrivial question since a renormalization group (RG) effect of the top quark can drive λ_H negative at certain high-energy scale, leading to an unbounded-from-below Higgs potential or a minimum that may be deeper than the EW vacuum. We will work out this question by solving RG equations with respect to the Higgs quartic couplings and the $U(1)_X$ gauge coupling. The one-loop β functions of those couplings are listed in Appendix A. In addition to the vacuum stability, we also take account of the perturbativity of the couplings. To be specific, we impose $\lambda_i(Q) < 4\pi$ ($i = H, H\Phi, \Phi$) and $g_X^2(Q) < 4\pi$ up to $Q = M_{\text{Pl}}$.

Fig. 7 shows the vacuum stability and the perturbativity constraints in the α - m_2 plane. We take $m_1 = 125$ GeV, $g_X = 0.05$, $M_X = m_2/2$ and $v_\Phi = M_X/(g_X Q_\Phi)$. The vacuum stability constraint is denoted by red line; i.e., the region above the red line is allowed for $\alpha > 0$, and it is the other way around for $\alpha < 0$. The perturbativity requirement is represented by blue line; i.e., the region below the blue line is allowed for $\alpha > 0$, and it is the other way around for $\alpha < 0$. For $\alpha < 0$, the region above the dotted black line is excluded by Eq. (4.1). Putting all together, for $\alpha > 0$ the region between the red and blue lines

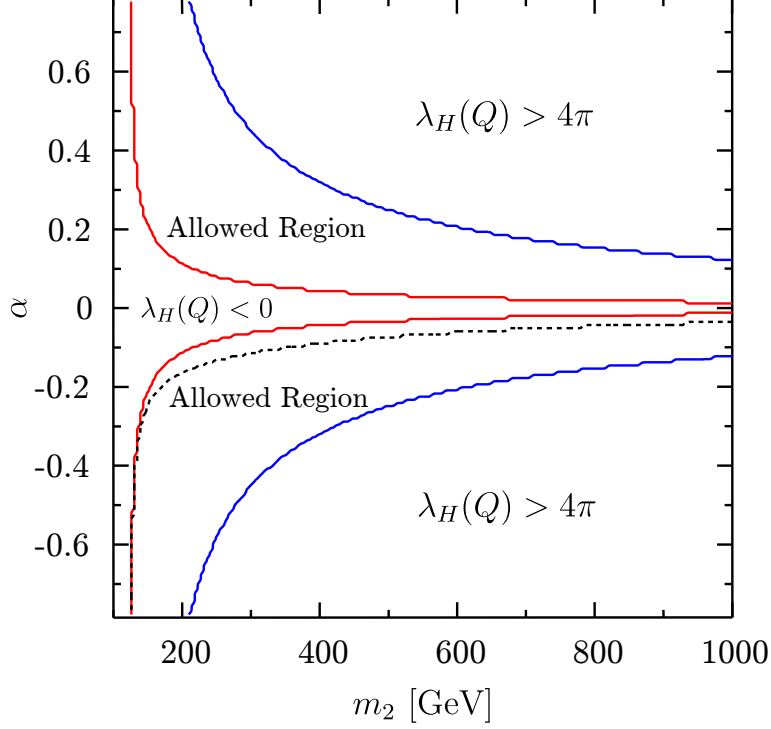


Figure 7. The vacuum stability and perturbativity constraints in the α - m_2 plane. We take $m_1 = 125$ GeV, $g_X = 0.05$, $M_X = m_2/2$ and $v_\Phi = M_X/(g_X Q_\Phi)$.

is allowed while for $\alpha < 0$ the region between the dotted black and blue lines is allowed. It should be noted that since the coefficient of $\lambda_{H\Phi}$ in β_{λ_H} is doubled in comparison with the real singlet case, the improvement of the vacuum stability by the increase of $\lambda_{H\Phi}$ or, equivalently α , is more effective. However, unlike the general Higgs potential involving explicit $U(1)_X$ breaking terms, the EW vacuum cannot be stable up to Planck scale if α is exactly zero.

In Fig. 8, we show the vacuum stability and perturbativity constraints in the M_X - m_2 plane. We fix $\alpha = 0.1$ varying g_X , i.e., $g_X = 0.1$ (Left Panel) and 0.5 (Right Panel). Once g_X is fixed, the small M_X is realized by a small v_Φ . In such a case, the large m_2 is possible only by a large λ_Φ since $m_2 \simeq \sqrt{2\lambda_\Phi} v_\Phi$ for a small α . This explains the regions excluded by $\lambda_\Phi(Q) > 4\pi$ in both plots. Indeed, the $g_X = 0.5$ case yields the severer constraints. As for the vacuum stability constraint, the change of g_X has little effect on it, which can be understood from the expression of β_{λ_H} , Eq. (A.2).

5 Conclusions

In this paper, we revisited the Higgs portal vector dark matter including the hidden sector Higgs field Φ that provides the vector dark matter mass. Including the hidden sector Higgs field makes the model renormalizable and unitary. The constraint from direct detection cross section (XENON100) still allows a large parameter space in this model. On the contrary to some claims that the Higgs portal dark matter model is strongly constrained

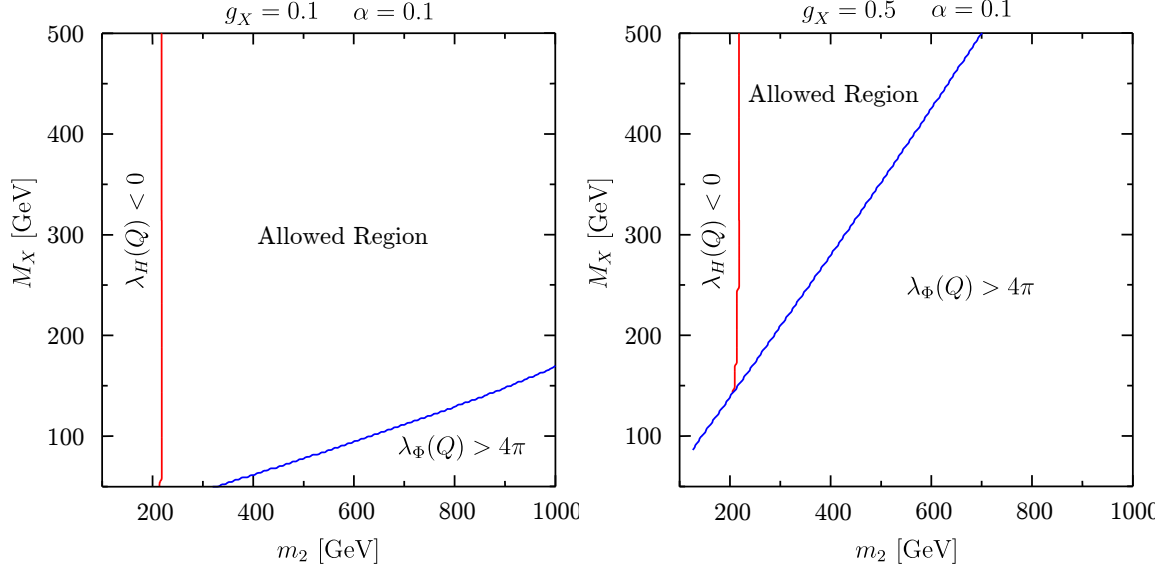


Figure 8. The vacuum stability and perturbativity constraints in the M_X - m_2 plane. We set $g_X = 0.1$ (Left Panel) and 0.5 (Right Panel) with being $\alpha = 0.1$.

by XENON100 data, we showed that the model is still viable. It is crucial to work with a model that is renormalizable, and not with effective lagrangian, as in the Higgs portal fermion DM model in Ref. [3, 8] Including the hidden sector Higgs field also improves the vacuum stability of the model for $m_H = 125$ GeV upto the Planck scale as in Ref. [8]. Our model can be tested at colliders by searching for the 2nd Higgs boson and/or the signal strength of the 125 GeV Higgs boson. It would take long in order to observe the 2nd Higgs boson since its signal strength is smaller than 0.3. In our model, r_i is universally suppressed relative to the SM case for all channels. This could be a useful criterion when the signal strengths of 125 GeV Higgs boson are measured with smaller uncertainties. If r_i is not universally suppressed or larger than one, then our model shall be excluded.

Acknowledgments

This work is supported in part by NRF Research Grant 2012R1A2A1A01006053 (PK and SB), and by SRC program of NRF Grant No. 20120001176 funded by MEST through Korea Neutrino Research Center at Seoul National University (PK). WIP is supported in part by Basic Science Research Program through the National Research Foundation of Korea(NRF) funded by the Ministry of Education, Science and Technology(2012-0003102).

A One-loop β functions of Higgs quartic couplings

The renormalization group equation and the β functions are given by

$$\frac{d\lambda(t)}{d\log(Q)} = \beta_\lambda, \quad (\text{A.1})$$

where

$$\beta_{\lambda_H} = \frac{1}{16\pi^2} \left[24\lambda_H^2 + \lambda_{H\Phi}^2 - 6y_t^4 + \frac{3}{8} \left\{ 2g_2^4 + (g_2^2 + g_1^2)^2 \right\} - \lambda_H \left\{ 3(3g_2^2 + g_1^2) - 12y_t^2 \right\} \right], \quad (\text{A.2})$$

$$\beta_{\lambda_{H\Phi}} = \frac{1}{16\pi^2} \left[2\lambda_{H\Phi}(6\lambda_H + 4\lambda_\Phi + 2\lambda_{H\Phi}) - \lambda_{H\Phi} \left\{ \frac{3}{2}(3g_2^2 + g_1^2) - 6y_t^2 + 6g_X^2 Q_\Phi^2 \right\} \right], \quad (\text{A.3})$$

$$\beta_{\lambda_\Phi} = \frac{1}{16\pi^2} \left[2(\lambda_{H\Phi}^2 + 10\lambda_\Phi^2 + 3g_X^4 Q_\Phi^4) - 12\lambda_\Phi g_X^2 Q_\Phi^2 \right], \quad (\text{A.4})$$

$$\beta_{g_X} = \frac{1}{16\pi^2} \frac{1}{3} g_X^3 Q_\Phi^2. \quad (\text{A.5})$$

References

- [1] S. Kanemura, S. Matsumoto, T. Nabeshima and N. Okada, Phys. Rev. D **82** (2010) 055026 [arXiv:1005.5651 [hep-ph]]; O. Lebedev, H. M. Lee and Y. Mambrini, Phys. Lett. B **707** (2012) 570 [arXiv:1111.4482 [hep-ph]]; A. Djouadi, O. Lebedev, Y. Mambrini and J. Quevillon, Phys. Lett. B **709** (2012) 65 [arXiv:1112.3299 [hep-ph]]. L. Lopez-Honorez, T. Schwetz and J. Zupan, Phys. Lett. B **716** (2012) 179 [arXiv:1203.2064 [hep-ph]].
- [2] Y. G. Kim, K. Y. Lee and S. Shin, JHEP **0805**, 100 (2008) [arXiv:0803.2932 [hep-ph]].
- [3] S. Baek, P. Ko and W. -I. Park, JHEP **1202** (2012) 047 [arXiv:1112.1847 [hep-ph]].
- [4] E. Aprile *et al.* [XENON100 Collaboration], Phys. Rev. Lett. **109** (2012) 181301 [arXiv:1207.5988 [astro-ph.CO]].
- [5] Z. Ahmed *et al.* [CDMS and EDELWEISS Collaborations], Phys. Rev. D **84**, 011102 (2011) [arXiv:1105.3377 [astro-ph.CO]].
- [6] G. Aad *et al.* [ATLAS Collaboration], Phys. Lett. B **716**, 1 (2012) [arXiv:1207.7214 [hep-ex]].
- [7] S. Chatrchyan *et al.* [CMS Collaboration], Phys. Lett. B **716**, 30 (2012) [arXiv:1207.7235 [hep-ex]].
- [8] S. Baek, P. Ko, W. -I. Park and E. Senaha, JHEP **1211**, 116 (2012) [arXiv:1209.4163 [hep-ph]].
- [9] O. Lebedev, Eur. Phys. J. C **72**, 2058 (2012) [arXiv:1203.0156 [hep-ph]].
- [10] J. Elias-Miro, J. R. Espinosa, G. F. Giudice, H. M. Lee and A. Strumia, JHEP **1206**, 031 (2012) [arXiv:1203.0237 [hep-ph]].
- [11] Work in preparation.
- [12] Y. Farzan and A. R. Akbarieh, JCAP **1210** (2012) 026 [arXiv:1207.4272 [hep-ph]].
- [13] E. Komatsu *et al.* [WMAP Collaboration], Astrophys. J. Suppl. **192**, 18 (2011) [arXiv:1001.4538 [astro-ph.CO]].
- [14] G. Belanger, F. Boudjema, P. Brun, A. Pukhov, S. Rosier-Lees, P. Salati and A. Semenov, Comput. Phys. Commun. **182** (2011) 842 [arXiv:1004.1092 [hep-ph]].
- [15] S. L. Glashow, J. Iliopoulos and L. Maiani, Phys. Rev. D **2**, 1285 (1970).
- [16] E. Aprile [XENON1T Collaboration], arXiv:1206.6288 [astro-ph.IM].